Inorg. Chem. **2007**, *46*, 1354–1360

Synthesis and Characterization of High-Quality ZnS, ZnS:Mn^{2+}, and ZnS:Mn^{2+}/ZnS (Core/Shell) Luminescent Nanocrystals

Zewei Quan,[†] Zhenling Wang,[†] Piaoping Yang,[†] Jun Lin,*[,†] and Jiye Fang[‡]

Key Laboratory of Rare Earth Chemistry and Physics, Changchun Institute of Applied Chemistry, Chinese Academy of Sciences, Changchun 130022, People's Republic of China, Graduate School of the Chinese Academy of Sciences, Beijing 100049, People's Republic of China, and Department of Chemistry, State University of New York at Binghamton, Binghamton, New York 13902-6000

Received October 7, 2006

High-quality ZnS, ZnS:Mn^{2+}, and ZnS:Mn^{2+}/ZnS (core/shell) nanocrystals (NCs) were synthesized via a high-boiling solvent process and characterized by X-ray diffraction (XRD), transmission electron microscopy (TEM), electron paramagnetic resonance (EPR), X-ray photoelectron spectroscopy (XPS), and photoluminescence (PL) spectra. The monodisperse ZnS NCs (size = 8 nm), which self-assembled into several micrometer-sized domains, were achieved by adopting poly(ethylene glycol) (PEG) in the reaction process (without using a size-selection process). The obtained ZnS:Mn^{2+} and ZnS:Mn^{2+}/ZnS core/shell NCs are highly crystalline and quasimonodisperse with an average particle size of 6.1 and 8.4 nm, respectively. All of the as-formed NCs can be well dispersed in hexane to form stable and clear colloidal solutions, which show strong visible emission (blue for ZnS and red-orange for ZnS:Mn^{2+} and ZnS:Mn^{2+}/ZnS) under UV excitation. The growth of a ZnS shell on ZnS:Mn^{2+} NCs, that is, the formation of ZnS:Mn^{2+}/ZnS core/shell NCs, resulted in a 30% enhancement in the PL intensity with respect to that of bare ZnS:Mn^{2+} NCs due to the elimination of the surface defects.

1. Introduction

Luminescent NCs have been extensively investigated during the past decade due to their application for various high-performance displays and devices.[1] Zinc sulfide (ZnS) is one of the most important wide band gap II−VI semiconductor materials, which has many valuable properties such as photoluminescence, electroluminescence, and photocatalytic properties. Recently, much attention has been paid to ZnS NCs due to the well-known quantum confinement. Using suitable surface-passivating agents such as thiols or surfactants that covalently bind to the surface atoms of the nanocrystallites, several groups have prepared free-standing ZnS NCs that are stable under normal atmospheric conditions.[2] By doping ZnS with different activating metal ions, one can tune the luminescence properties to a large extent.[3] Among them, manganese-doped ZnS (ZnS:Mn^{2+}) NCs have been receiving much attention due to their promising application in optoelectronic devices.[4]

The self-assembled NCs, including three-dimensional NC superlattices (NCSs) and two-dimensional NC arrays (NCAs), have attracted much attention due to their unique importance in many fields such as integrated circuits, information storage devices, light-harvesting structures, and thin-film display devices.[5] Usually, the self-assembly of NCs is the combination of particle uniformity and carefully controlled growth environment that permits the formation of ordered assemblies, as demonstrated for many natural systems.[6] Various

* To whom correspondence should be addressed. E-mail: jlin@ciac.jl.cn.
[†] Changchun Institute of Applied Chemistry, and Graduate School of the Chinese Academy of Sciences.
[‡] State University of New York at Binghamton.

(1) (a) Chander, H. *Mater. Sci. Eng., R:* **2005**, *49*, 113. (b) Steckel, J. S.; Zimmer, J. P.; Coe-Sullivan, S.; Stott, N. E.; Bulovic, V.; Bawendi, M. G. *Angew. Chem., Int. Ed.* **2004**, *43*, 2154. (c) Talapin, D. V.; Rogach, A. L.; Kornowski, A.; Haase, M.; Weller, H. *Nano Lett.* **2001**, *1*, 207. (d) Eychmüller, A. *J. Phys. Chem. B* **2000**, *104*, 6514.

(2) (a) Nanda, J.; Sapra, S.; Sarma, D. D. *Chem. Mater.* **2000**, *12*, 1018. (b) Nakaoka, Y.; Nosaka, Y. *Langmuir* **1997**, *13*, 708. (c) Kortan, A. R.; Hull, R.; Opila, R. L.; Bawendi, M. G.; Steigerwald, M. L.; Carroll, P. J.; Brus, L. E. *J. Am. Chem. Soc.* **1990**, *112*, 1327.

(3) (a) Ge, J. P.; Wang, J. W.; Zhang, H. X.; Wang, X.; Peng, Q.; Li, Y. D. *Adv. Funct. Mater.* **2005**, *15*, 303. (b) Chen, W.; Joly, A. G.; Zhang, J. Z. *Phys. Rev. B* **2001**, *64*, 041202. (c) Yang, H. S.; Holloway, P. H.; Ratna, B. B. *J. Appl. Phys.* **2003**, *93*, 586. (d) Do, Y. R.; Kim, Y. C.; Cho, S. H.; Ahn, J. H.; Lee, J. G. *Appl. Phys. Lett.* **2003**, *82*, 4172. (e) Adams, M.; Mascher, P.; Kitai, A. H. *Appl. Phys. A: Mater. Sci. Process.* **1995**, *61*, 217.

(4) (a) Karara, N.; Raj, S.; Singh, F. *J. Cryst. Growth* **2004**, *268*, 585. (b) Chung, J. H.; Ah C. S.; Jang, D. J. *J. Phys. Chem. B* **2001**, *105*, 4128. (c) Suyver, J. F.; Wuister, S. F.; Kelly, J. J.; Meijerink, A. *Nano Lett.* **2001**, *1*, 429.

10.1021/ic061917n CCC: $37.00 © 2007 American Chemical Society
Published on Web 01/23/2007

methods have been developed to produce monodisperse NCs which are often defined as NCs with a standard deviation of $\sigma \leq 5\%$ in diameter.[7] Although many monodisperse NC systems such as semiconductors[8] and metals[9] have been prepared through colloidal chemistry, they mostly focus on adjustments of general experimental conditions such as precursors, ligands, and reaction temperature, which are usually complicated and need further size-selection processes. A facile process without size selection to obtain monodisperse NCs is highly desired.

On the other hand, a large portion of atoms are located on or near the surface of NCs due to their high surface-to-volume ratios, which have significant effects on their structural and optical properties.[10] Hence, the surface chemistry of luminescent II−VI semiconductor NCs has been extensively studied to improve the luminescent characteristics such as quantum efficiency and photostability.[11] For inorganically passivated (or core/shell) NCs, the luminescent properties can be sufficiently improved by heteroepitaxially growing an inorganic shell of a wider band gap semiconductor around the particles.[1c,12] However, due to its wide band gap (3.67 eV for bulk ZnS[13]), it is difficult to find another suitable shell material with a wider band gap to form the so-called core/shell NCs and, therefore, improve the luminescent properties. Furthermore, for the general core/shell NCs, the mismatch between core and shell lattice constants induces strain at their interface, which causes the decrease of quantum yield and stability when the shell thickness exceeds a certain amount. Cao and co-workers prepared ZnS:Mn^{2+} and ZnS:Mn^{2+}/ZnS core/shell NCs by the reverse micelle method and observed the obvious enhancement of the PL intensity after the formation of a ZnS shell on ZnS:Mn^{2+}, but the exact size, morphology, and homogeneity of these nanocrystals were unknown because neither SEM nor TEM images were provided therein.[14] Moreover, to get well-defined and optimized properties, it is necessary that the synthesized nanoparticles possess a narrow size distribution, high crystallinity, and low defect density.

In this paper, we report the synthesis and luminescent properties of monodisperse and high-quality ZnS, ZnS:Mn^{2+}, and ZnS:Mn^{2+}/ZnS (core/shell) NCs via a high-boiling solvent process. Highly monodisperse ZnS NCs were obtained by adding poly(ethylene glycol) (PEG) to the reaction system (without a size-selective process). These monodisperse ZnS NCs can be self-assembled into closely packed and ultra-large-range (to several micrometers), ordered 2D arrays on the carbon-coated copper grid. To our knowledge, this is the best result of ZnS NCs' self-assembly in such a large domain among the reported literature. As for the ZnS:Mn^{2+} NCs system, ZnS was chosen to overcoat it to form ZnS:Mn^{2+}/ZnS core/shell NCs, which could eliminate surface defects and also avoid the lattice mismatch between the core and shell materials. Finally, the growth of a ZnS shell on ZnS:Mn^{2+} NCs resulted in a 30% enhancement of the PL intensity with respect to that of the bare ZnS:Mn^{2+}.

2. Experimental Section

Materials. $ZnCl_2$ (98.0%, analytical reagent), $MnCl_2$ (99.0%, AR), poly(ethylene glycol) (molecular weight = 10 000, AR), and sulfur powder (99.5%, chemically pure) were purchased from Beijing Beihua Chemicals Co., Ltd. Oleylamine (70%, technical grade) and trioctylphosphine oxide (TOPO, 90%, technical grade) were purchased from Aldrich. All of the materials were used without further purification.

Synthesis of ZnS NCs. The ZnS NCs were prepared via a high-boiling solvent process. First, $ZnCl_2$ (2 mmol), PEG (2.5 g), and oleylamine (10 mL) were mixed together under vacuum at 170 °C for 1 h to form a clear solution (solution 1). Then, sulfur (6 mmol) was dissolved in 3 mL of oleylamine at 50 °C to form another solution (solution 2). Solution 2 was injected into solution 1 at 170 °C, and then, the temperature was rapidly elevated to 290 °C and held for 1 h under agitation in an argon atmosphere and then cooled to room temperature. ZnS NCs were obtained by adding excess ethanol to the solutions and separating by centrifugation. After being washed thoroughly with ethanol, the yielded precipitates could be redispersed in hexane to form a stable and clear colloidal solution.

Synthesis of ZnS:Mn^{2+} and ZnS:Mn^{2+}/ZnS Core/Shell NCs. The ZnS:Mn^{2+} and ZnS:Mn^{2+}/ZnS core/shell NCs were also prepared via a high-boiling solvent process with TOPO instead of PEG in the reaction systems.[15] In this system, TOPO (2.5 g) was adopted to replace PEG due to the weak coordination ability of PEG for Zn^{2+} and Mn^{2+}, (As a comparison, the results of ZnS:Mn^{2+} and ZnS:Mn^{2+}/ZnS core/shell NCs prepared with oleylamine

(5) (a) Wu, Q. Z.; Cao, H. Q.; Zhang, S. C.; Zhang, X. R. *Inorg. Chem.* **2006**, *45*, 4586. (b) Cho, Y. H.; Cho, G.; Lee, J. S. *Adv. Mater.* **2004**, *16*, 1814. (c) Geissler, M.; Xia, Y. *Adv. Mater.* **2004**, *16*, 1249. (d) Achermann, M.; Petruska, M. A.; Crooker, S. A.; Klimov, V. I. *J. Phys. Chem. B* **2003**, *107*, 13782. (e) Wang, X.; Summers, C. J.; Wang, Z. L. *Nano Lett.* **2004**, *4*, 423. (f) Murray, C. B.; Kagan, C. R.; Bawendi, M. G. *Science* **1995**, *270*, 1335. (g) Motte, L.; Billoudet, F.; Lacaze, E.; Pileni, M. P. *Adv. Mater.* **1996**, *8*, 1018. (h) Ohara, P. C.; Heath, J. R.; Gelbart, W. M. *Angew. Chem., Int. Ed.* **1997**, *36*, 1078. (i) Korgel, B. A.; Fitzmaurice, D. *Adv. Mater.* **1998**, *10*, 661. (j) Kiely, C. J.; Fink, J.; Brust, M.; Bethell, D.; Schiffrin, D. J. *Nature* **1998**, *396*, 444. (k) Taleb, A.; Silly, F.; Gusev, O.; Charra, F.; Pileni, M. P. *Adv. Mater.* **2000**, *12*, 119. (l) Ngo, T.; Pileni, M. P. *Adv. Mater.* **2000**, *12*, 276.
(6) Murray, C. B; Kagan, C. R.; Bawendi, M. G. *Annu. Rev. Mater. Sci.* **2000**, *30*, 545.
(7) Overbeek, J. T. G. *Adv. Colloid Interface Sci.* **1982**, *15*, 251.
(8) (a) Hines, M. A.; Guyot-Sionnest, P. *J. Phys. Chem. B* **1998**, *102*, 3655. (b) Micic, O. I.; Sprague, J. R.; Curtis, C. J.; Jones, K. M.; Nozik, A. J. *J. Phys. Chem.* **1994**, *98*, 4966. (c) Guzelian, A. A.; Katari, J. E. B.; Kadavanich, A. V.; Banin, U.; Hamad, K.; Juban, E.; Alivisatos, A. P.; Wolters, R. H.; Arnold, C. C.; Heath, J. R. *J. Phys. Chem.* **1996**, *100*, 7212. (d) Guzelian, A. A.; Banin, U.; Kadavanich, A. V.; Peng, X.; Alivisatos, A. P. *Appl. Phys. Lett.* **1996**, *69*, 1432.
(9) (a) Taleb, A.; Petit, C.; Pileni, M. P. *Chem. Mater.* **1997**, *9*, 950. (b) Motte, L.; Billoudet, F.; Lacaze, E.; Pileni, M. P. *Adv. Mater.* **1996**, *8*, 1018. (c) Petit, C.; Taleb, A.; Pileni, M. P. *J. Phys. Chem. B* **1999**, *103*, 1805.
(10) Alivisatos, A. P. *J. Phys. Chem.* **1996**, *100*, 13226.
(11) (a) Yang, H.; Holloway, P. H. *Adv. Funct. Mater.* **2004**, *14*, 152. (b) Peng, X.; Schlamp, M. C.; Kadavanich, A. V.; Alivisatos, A. P. *J. Am. Chem. Soc.* **1997**, *119*, 7019. (c) Katari, J. E. B.; Colvin, V. L.; Alivisatos, A. P. *J. Phys. Chem.* **1994**, *98*, 4109. (d) Nirmal, M.; Brus, L. *Acc. Chem. Res.* **1999**, *32*, 407.
(12) (a) Kuno, M.; Lee, J. K.; Dabbousi, B. O.; Mikulec, F. V.; Bawendi, M. G. *J. Chem. Phys.* **1997**, *106*, 9869. (b) Hines, M. A.; Guyot-Sionnest, P. *J. Phys. Chem.* **1996**, *100*, 468.
(13) Sapra, S.; Prakash, A.; Ghangrekar, A.; Periasamy, N.; Sarma, D. D. *J. Phys. Chem. B* **2005**, *109*, 1663.
(14) Cao, L. X.; Zhang, J. H.; Ren, S. L.; Huang, S. H. *Appl. Phys. Lett.* **2002**, *80*, 4300.
(15) Joo, J.; Na, H. B.; Yu, T.; Kim, Y. W.; Wu, F.; Zhang, J. Z.; Hyeon, T. *J. Am. Chem. Soc.* **2003**, *125*, 11100.

Scheme 1. Schematic Diagram for the Formation of ZnS:Mn^{2+} (A) and ZnS:Mn^{2+}/ZnS (B) Core/Shell NCs

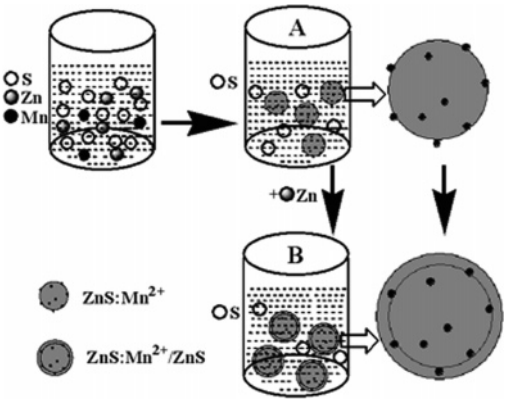

and PEG are shown in Figure S1 of Supporting Information, which are not as good as those obtained by using oleylamine and TOPO as the capping ligands, as reported in this paper.) The doping concentration of Mn^{2+} was 10 mol % of Zn^{2+} in ZnS. The other synthesis procedures are the same as those for the synthesis of ZnS NCs. After the first step, the resulting product (sample A) is a ZnS:Mn^{2+} deep-yellow colloidal solution with excess S. The growth of a ZnS shell on ZnS:Mn^{2+} was achieved after the Zn^{2+} precursor solution was injected into the ZnS:Mn^{2+} colloidal solution (with the presence of excess S) at 50 °C; then, the reaction temperature was increased to 290 °C and maintained for another 1 h. The solution turned out to be clear (slightly yellow), indicative of the decrease of the S concentration and, therefore, of the formation of the ZnS shell (sample B). Finally, the ZnS:Mn^{2+} and ZnS:Mn^{2+}/ZnS core/shell NCs were obtained by adding excess ethanol to the corresponding solutions (samples A and B, respectively). The following procedures are the same as those for the synthesis of ZnS NCs, as stated above. The whole reaction process is shown in Scheme 1.

Characterization. X-ray diffraction (XRD) was carried out on a Rigaku-Dmax 2500 diffractometer with Cu Kα radiation (λ = 0.15405 nm) (40 kV, 200 mA). TEM images were obtained using a JEOL 2010 transmission electron microscope operating at 200 kV. Samples for TEM were prepared by depositing a drop of the samples dispersed in hexane onto a carbon grid. The excess liquid was wicked away with filter paper, and the grid was dried in air. The X-ray photoelectron spectra (XPS) were taken on a VG ESCALAB MK II electron energy spectrometer using Mg Kα (1253.6 eV) as the X-ray excitation source. Electron paramagnetic resonance (EPR) measurements were performed using an X-band (9.440 GHz) JES-FE3AX spectrometer (JEOL) at 293 K. Cylindrical quartz tube containers were used to insert the powders into the microwave cavity. The excitation and emission spectra were taken on an F-4500 spectrophotometer equipped with a 150 W xenon lamp as the excitation source. The luminescence lifetimes were measured with a Lecroy Wave Runner 6100 digital oscilloscope (1 GHz) using a 266 nm laser wavelength (pulse width = 4 ns) from a Nd:YAG as the excitation source. The spectra and lifetimes were both obtained from samples dispersed in hexane solutions. All of the measurements were performed at room temperature.

3. Results and Discussion

3.1. Formation, Structure, and Morphology of the Nanocrystals. XRD. Figure 1 shows the XRD patterns of the as-prepared ZnS (a), ZnS:Mn^{2+} (b), and ZnS:Mn^{2+}/ZnS (c) core/shell NCs. Vertical bars indicate a standard cubic bulk ZnS peak position from JCPDS No. 77−2100. It is obvious that all of the XRD peaks of the NCs can be indexed as the cubic zinc blende structure, which is consistent with the values in the standard card. It can be seen that XRD patterns are broadened with three main peaks corresponding to the (111), (220), and (311) planes. The broadening of the XRD lines is attributed to the NC nature of the samples and can be used to estimate the average crystallite size by Scherer's formula, which are 8.1 nm (ZnS), 6.3 nm (ZnS:Mn^{2+}), and 8.2 nm (ZnS:Mn^{2+}/ZnS), close to those observed from TEM images (see the next TEM part). The calculated lattice constant of pure ZnS NCs, a = 0.5415 nm, is the same as the value from the standard card (a = 0.5415 nm). However, as for ZnS:Mn^{2+} and ZnS:Mn^{2+}/ZnS NCs, we observe the slight increase in the lattice constant, that is, a = 0.5419 and 0.5418 nm, respectively. This is probably caused by the substitution of Zn^{2+} by Mn^{2+} since the diameter of Mn^{2+} (0.83 nm) is larger than that of Zn^{2+} (0.74 nm).[16]

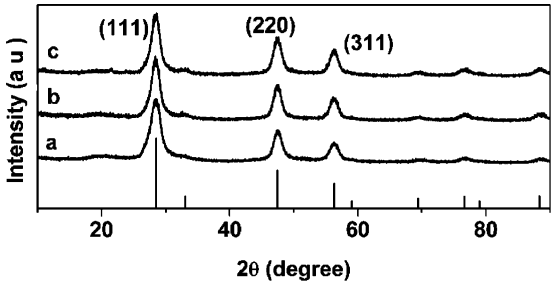

Figure 1. XRD patterns of pure ZnS (a), ZnS:Mn^{2+} (b), and ZnS:Mn^{2+}/ZnS (c) core/shell NCs as well as the standard data for ZnS (vertical bars, JCPDS card No. 77−2100).

TEM. Figure 2 shows the TEM results of the as-prepared ZnS NCs. A typical TEM image in low magnification is shown in Figure 2a. It can be seen that the resultant ZnS NCs are uniform spherical-shaped particles, 8 nm in diameter, and with a very narrow size distribution (the particle size distribution histogram is shown in the inset of Figure 2c). These monodisperse ZnS NCs are self-assembled into a closely packed hexagonal array with one particle surrounded symmetrically by the other six particles. Even better ordered 2D arrays of ZnS NCs with domain sizes as large as several micrometers can be also obtained (Supporting Information, Figure S2). The formation of the hexagonal 2D ZnS nanoarray can be attributed to the equilibrium built between the van der Waals attractive forces and the steric repulsions from the capping ligand (oleylamine).[17] Because these forces are isotropic, this equilibrium yields a compact organization in the hexagonal 2D network. A high-resolution TEM (HRTEM) image of the ZnS NCs is shown in Figure 2b. It demonstrates the high crystallinity of the ZnS NCs, and the distances (0.310 nm) between the adjacent lattice fringes are the interplanar distances of ZnS (111) plane, agreeing well with the (111) d spacing of the literature value, 0.312 nm (JCPDS No. 77−2100). The selected area electron

(16) Shannon, R. D. *Acta Crystallogr., Sect. A* **1976**, *32*, 751.
(17) Li, Y. C.; Li, X. H.; Yang, C. H.; Li, Y. F. *J. Phys. Chem. B* **2004**, *108*, 16002.

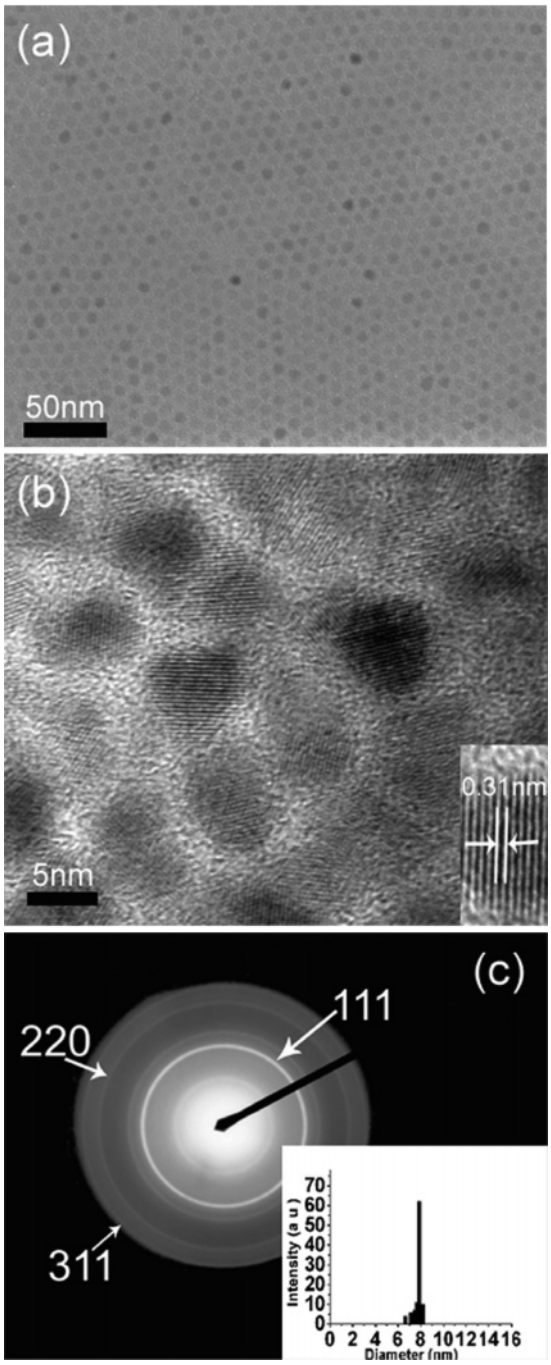

Figure 2. TEM image (a), HRTEM image (b), and selected area electron diffraction (SAED) pattern (c, inset: particle size distribution histogram) of ZnS NCs.

diffraction (SAED) pattern (Figure 2c) indicates that the ZnS NCs possess high crystallinity and a cubic structure, in which the three diffraction rings are perfectly indexed to the same positions as those from bulk ZnS.

The addition of PEG in the experimental process seems to play a key role in obtaining the highly monodisperse ZnS NCs. As a comparison, the TEM image of ZnS NCs prepared without PEG in the reaction process is shown in Figure S3 (Supporting Information). Obviously, the uniformity and monodispersity of this sample are not as good as those in the presence of PEG (Figures 2a and S2). Here, we introduce the classic studies by LaMer and Dinegar, that is, the production of monodisperse colloids requires a temporally discrete nucleation event followed by slower controlled growth on the existing nuclei to explain this result.[18] In our experiments, rapid injection of the S precursor to the reaction vessel at a high temperature (170 °C) raises the S precursor concentration above the nucleation threshold, and then, a short nucleation burst partially relieves the supersaturation.[6] Reiss pointed out that, if the percentage of NCs' growth during the nucleation period is small compared with subsequent growth, the NCs can become more uniform over time.[19] As for the oleylamine ligand in our system, the nucleation rate is very fast, which is essential to the preparation of monodisperse NCs. While, for the PEG, the multihydroxy-containing compound can also function as a ligand, the combination for the metal ions is relatively very weak compared with oleylamine, and therefore, the effect of PEG in the nucleation process can almost be ignored. During the growth process, the system is still supersaturated; consequently, the process of the growth of stable nuclei to form discrete particles can proceed by diffusion of molecularly dissolved ZnS to the nuclei. Further deposition of ZnS on the existing nuclei is a natural process and occurs spontaneously. In the formation mechanism of monodisperse particles originally proposed by LaMer,[18] the growth rate depends mainly on three factors, namely, the number of nuclei which are to grow, the total amount of diffusible nuclei, and their diffusion coefficient in the medium. It is obvious that the diffusion depends inversely on the viscosity of the reaction medium. In the present synthetic procedure, the addition of PEG in the solution does not have any effect on the first two factors but has an obvious effect on the viscosity of the reaction medium due to its large molecular weight. The viscosity of the reaction medium increases greatly in the presence of PEG. Thus, the diffusion rate of ZnS nuclei decreases significantly, which slows down the diffusion rate of dissolvable ZnS to the crystal surfaces of the as-formed nuclei and ensures that the diffusion process becomes the rate-control step during the crystal growth procedure.[20] A model for the growing process is schematically shown in Figure 3. Compared with the formation of ZnS NCs with less uniformity through route (a) (without PEG), the long chain structure of PEG in solution acts like a barrier for the fast movement of solutes, promoting the homogeneous growth of the crystal nuclei and finally the formation of monodisperse NCs (Figure 3b). In order to further check the function of PEG for the formation of monodisperse NCs, CdS NCs were prepared in a similar way as that for ZnS NCs (Supporting Information). It is observed that the CdS NCs obtained in the presence of PEG are more uniform than those without PEG (Supporting Information, Figure S4). Note that similar results were also reported for the formation of monodisperse Bi_2O_3 NCs by the utilization of PEG with the proper molecular weight, which has been explained in the same way as described previously.[20]

(18) La Mer, V. K.; Dinegar, R. H. *J. Am. Chem. Soc.* **1950**, *72*, 4847.
(19) Reiss, H. *J. Chem. Phys.* **1951**, *19*, 482.
(20) Li, W. *Mater. Chem. Phys.* **2006**, *99*, 174.

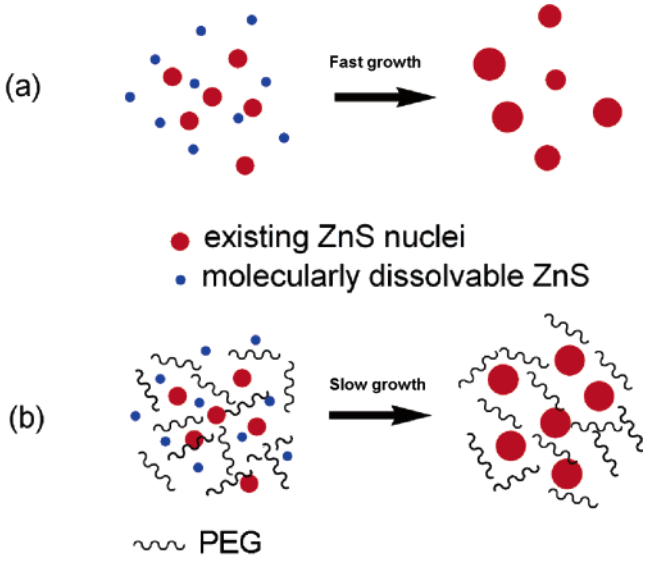

Figure 3. A model diagram for the formation of ZnS NCs without PEG (a) and in the presence of PEG (b).

However, it seems that the PEG only works well in obtaining high-quality and monodisperse ZnS NCs, in which only one kind of cation (Zn^{2+}) is present in the reaction system. When more than one kind of cation (Zn^{2+}, Mn^{2+}) is present in the reaction system, the uniformity of the obtained ZnS:Mn^{2+} and ZnS:Mn^{2+}/ZnS NCs (see the TEM images in Supporting Information, Figure S1) is not as good as that of pure ZnS NCs (Figures 1a and S2). The reason for this is not very clear at this stage, but most probably, it is related to different nucleation rates of different cations. As a result, in the preparation of ZnS:Mn^{2+} and ZnS:Mn^{2+}/ZnS core/shell NCs, we employed TOPO (a well-known capping ligand for metal ions) instead of PEG in the reaction process to obtain the NCs with good morphology and uniformity. Figure 4 shows TEM images of ZnS:Mn^{2+} (a, c) and ZnS:Mn^{2+}/ZnS core/shell (b, d) NCs together with their particle size distribution histograms (e, f). ZnS:Mn^{2+} NCs show spherical morphology and a relatively narrow size distribution with the tendency to form a self-organized monolayer. After the growth of the ZnS shell, it shows no difference with ZnS:Mn^{2+} NCs except for their average diameter. Due to the growth of the ZnS shell on ZnS:Mn^{2+} NCs, the average size (8.4 nm) for ZnS:Mn^{2+}/ZnS core/shell NCs is larger than that (6.1 nm) of the core ZnS:Mn^{2+} NCs, which is clearly shown in their particle size distribution histograms. The difference between them means that the shell thickness is around 1.15 nm. The particle size values observed from TEM images are basically consistent with those estimated from XRD. The core and the shell of the nanoparticles, however, have similar electron densities and lattice parameters, and the image contrast cannot be used to distinguish the shell and core. High-resolution TEM images of ZnS:Mn^{2+} (Figure 4c) and ZnS:Mn^{2+}/ZnS core/shell (Figure 4d) NCs indicate that as-synthesized NCs are highly crystalline, and the distances between the adjacent lattice fringes, measured as 0.320 nm, agree well with the literature value for the (111) *d* spacing, 0.312 nm (JCPDS No. 77−2100).

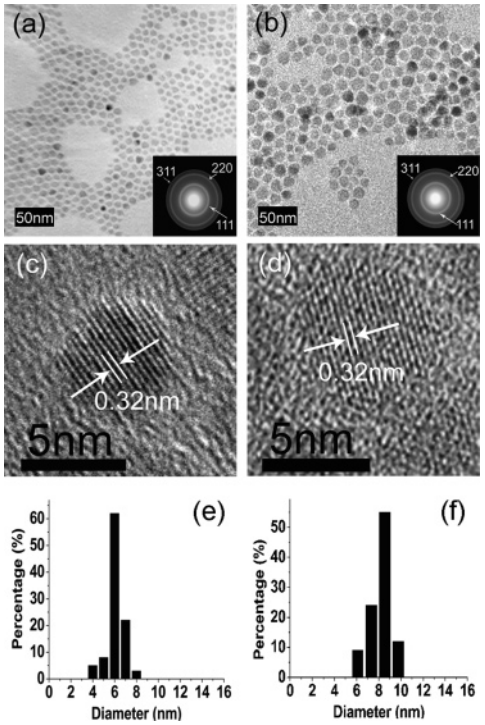

Figure 4. TEM images of ZnS:Mn^{2+} (a, c: high resolution) and ZnS:Mn^{2+}/ZnS (b, d: high resolution) core/shell NCs. The corresponding selected area electron diffraction (SAED) patterns are shown in the inset of (a) and (b); (e) and (f) are their particle size distribution histograms, respectively.

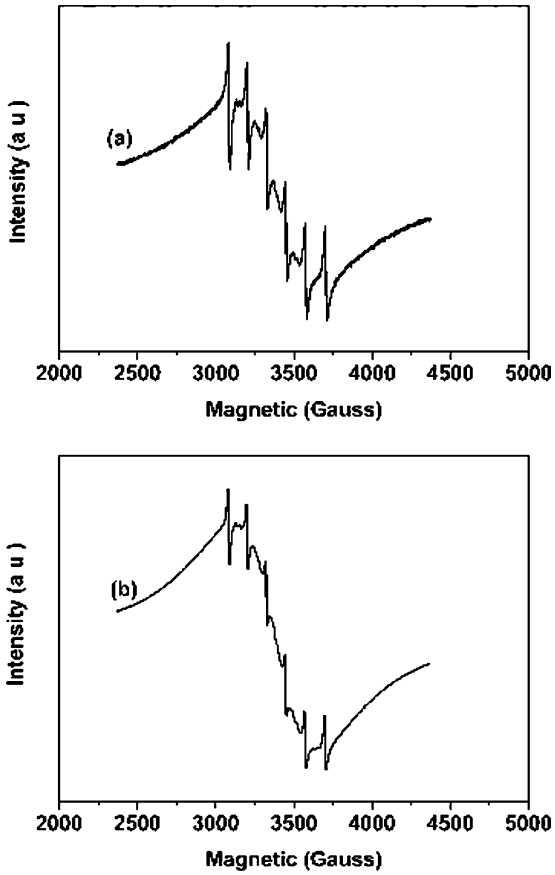

Figure 5. EPR spectra of ZnS:Mn^{2+} (a) and ZnS:Mn^{2+}/ZnS (b) core/shell NCs.

EPR. The growth of the ZnS shell on ZnS:Mn^{2+} NCs can be confirmed by EPR spectra, to some extent. Figure 5 shows

the EPR spectra of ZnS:Mn^{2+} (a) and ZnS:Mn^{2+}/ZnS core/shell (b) NCs. Both EPR spectra consist of a broad curve and six lines of sharp splitting. The broad curve is caused by the electron spin−spin interactions ($1/2 \rightarrow -1/2$) of the isolated Mn^{2+} ions in the ZnS:Mn^{2+} NCs, in which a symmetric Lorentzian line of the broad curve is observed since the sample size is smaller than the skin depth.[21] The six lines are due to the hyperfine interaction with the ^{55}Mn nuclear spin ($I = 5/2$), which indicates that the Mn^{2+} ions have entered the ZnS host lattices.[22] This hyperfine structure shows the electron spin−nuclear spin interactions in an isolated Mn^{2+} ion. As the Mn^{2+} ion is affected by other Mn^{2+} ions that are randomly distributed around it, the Mn−Mn interactions should result in a reduction of the electron spin−nuclear spin interactions in an individual Mn ion.[21] This phenomenon is observed after the formation of the ZnS shell on the ZnS:Mn^{2+} NCs. The signals from the EPR spectrum of the ZnS:Mn^{2+} NCs show six well-resolved peaks, while those for ZnS:Mn^{2+}/ZnS NCs have a poorly resolved six line structure because some Mn^{2+} ions near the surface of ZnS:Mn^{2+} are shielded by the additional ZnS shell layers.[23]

XPS. To further characterize the as-obtained products, we carried out XPS to investigate the surface compositions and chemical state of ZnS:Mn^{2+} and ZnS:Mn^{2+}/ZnS core/shell NCs, and the results are shown in Figure 6a and 6b, respectively. Since XPS is a surface-sensitive technique, its spectra should be dominated by the shell. In our system, the ZnS:Mn^{2+} and ZnS:Mn^{2+}/ZnS core/shell NCs are capped with oleylamine, and therefore, the XPS lines of C 1s and O 1s are present in Figure 6a and 6b. The intensity of the Zn $2p_{3/2}$ peak in ZnS:Mn^{2+}/ZnS core/shell NCs is obviously higher than that of the ZnS:Mn^{2+} NCs, which can explain the formation of the ZnS shell to some extent. It should be noted that the Mn XPS line (at ~640 eV), marked with dashed line in Figure 6, does not appear in both samples due to its low concentration (on the surface of the NCs). This phenomenon has also been observed in many other types of manganese-doped NCs.[11a,24]

3.2. Photoluminescence (PL) of the Nanocrystals. Figure 7 displays the photoluminescence excitation (a) and emission (b) spectra of as-prepared ZnS NCs dispersed in a hexane solution. The photoluminescence of ZnS NCs is intricate because it is sensitive to the synthesis conditions and crystal sizes and shapes.[17] In the present work, the emission spectrum obtained under 401 nm excitation is a broad band centered at 462 nm. We attribute this photoluminescence to the trapped surface state's emission, which has been studied extensively.[25] The visual image of the ZnS NCs that shows a strong blue emission is obtained under a 365 nm UV light irradiation (the inset of Figure 7). Generally, the most

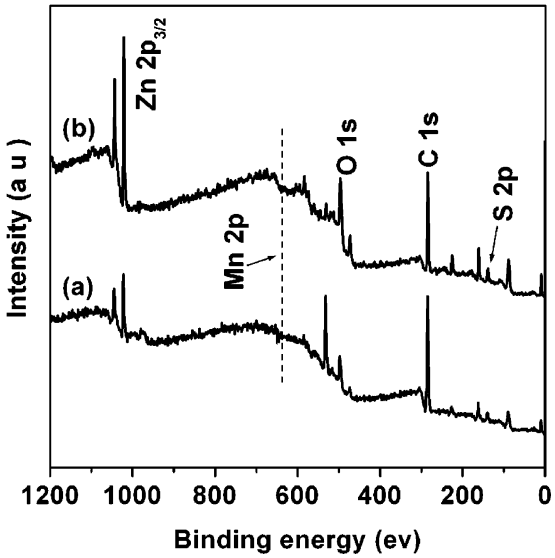

Figure 6. XPS of ZnS:Mn^{2+} (a) and ZnS:Mn^{2+}/ZnS (b) core/shell NCs.

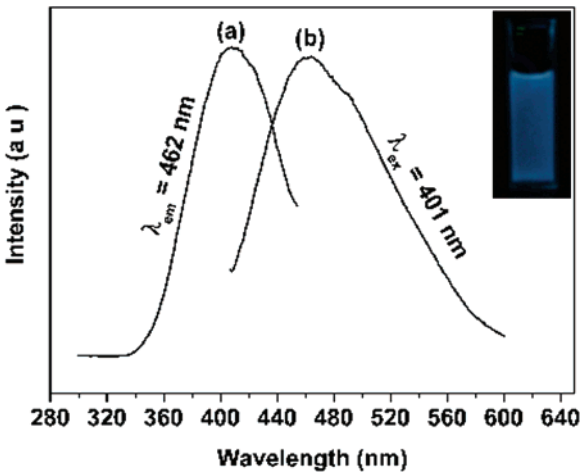

Figure 7. PL excitation and emission spectra of ZnS NCs. The visual image of ZnS NCs under a 365 nm UV lamp irradiation is shown in the inset.

efficient excitation wavelength for the ZnS NCs is shorter than the band gap excitation of bulk ZnS (330 nm) due to the size-dependent quantum confinement effects. However, in our excitation spectrum (monitored with an emission wavelength of 462 nm), it shows a broad band with a maximum at 401 nm, which is much longer than the band gap excitation wavelength. We think that this excitation can be attributed to the surface defects in the ZnS NCs due to their high surface-to-volume ratio.

Figure 8 demonstrates the photoluminescence emission spectra of ZnS:Mn^{2+} (a) and ZnS:Mn^{2+}/ZnS (b) core/shell NCs. Upon excitation into the band gap of ZnS using 310 nm UV light, the obtained emission spectra for both ZnS:Mn^{2+} and ZnS:Mn^{2+}/ZnS core/shell NCs consist of a weak band at 460 nm and a strong band at 580 nm. The former is attributed to the trap state's emission of ZnS NCs,[12c] and

(21) Ji, T. H.; Jian, W. B.; Fang, J. Y. *J. Am. Chem. Soc.* **2003**, *125*, 8448.
(22) Norris, D. J.; Yao, N.; Charnock, F. T.; Kennedy, T. A. *Nano Lett.* **2001**, *1*, 3.
(23) Kennedy, T. A.; Glaser, E. R.; Klein, P. B.; Bhargava, R. N. *Phys. Rev. B* **1995**, *52*, R14356.
(24) (a) Yang, H.; Holloway, P. H. *Appl. Phys. Lett.* **2003**, *82*, 1965. (b) Ethiraj, A. S.; Hebalkar, N.; Kulkarni, S. K.; Pasricha, R.; Urban, J.; Dem, C.; Schmitt, M.; Kiefer, W.; Weinhardt, L.; Joshi, S.; Fink, R.; Heske, C.; Kumpf, C.; Umbach, E. *J. Chem. Phys.* **2003**, *118*, 8945.
(25) (a) Weller, H. *Angew. Chem., Int. Ed. Engl.* **1993**, *32*, 41. (b) Steigerwald, M. L.; Brus, L. E. *Acc. Chem. Res.* **1990**, *23*, 183. (c) Cizeron, J.; Pileni, M. P. *J. Phys. Chem. B* **1997**, *101*, 8887. (d) Nand, J.; Sapra, S.; Sarma, D. D.; Chandrasekharan, N.; Hodes, G. *Chem. Mater.* **2000**, *12*, 1018.

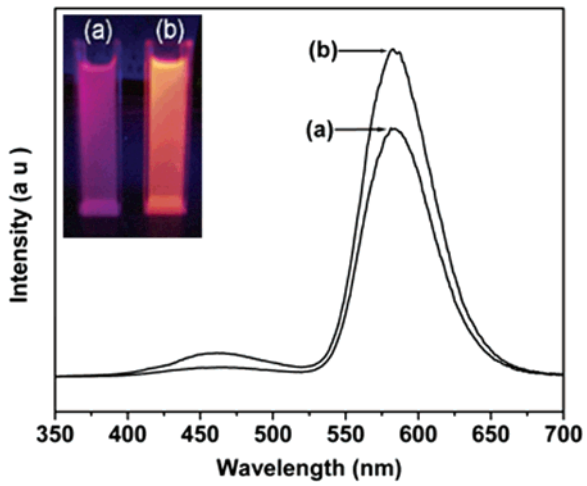

Figure 8. PL emission spectra of ZnS:Mn^{2+} (a) and ZnS:Mn^{2+}/ZnS (b) core/shell NCs. Visual images of the samples under a 365 nm UV lamp irradiation are shown in the inset of the emission spectra (note that the colloid of the ZnS:Mn^{2+}/ZnS (b) core/shell NCs is much brighter than that of the ZnS:Mn^{2+} (a) NCs).

the latter is attributed to the emission of Mn^{2+} that corresponds to the $^4T_1 \rightarrow {}^6A_1$ transition within the $3d^5$ configuration of Mn^{2+}.[22] Obviously, the ZnS:Mn^{2+}/ZnS core/shell NCs exhibit increased photoluminescence intensity (integrated area) by 30% with respect to that of ZnS:Mn^{2+} NCs, which can also be seen clearly in the visual images (inset) of ZnS:Mn^{2+} (a) and ZnS:Mn^{2+}/ZnS (b) core/shell NCs under a UV lamp providing 365 nm UV light irradiation. The lifetime of the Mn^{2+} $^4T_1 \rightarrow {}^6A_1$ emission in the ZnS:Mn^{2+}/ZnS core/shell NCs is 1.74 ms, which is slightly longer than that (1.70 ms) of Mn^{2+} in ZnS:Mn^{2+} NCs. In ZnS:Mn^{2+} NCs, the excited Mn^{2+} 5d states are primarily populated by an energy transfer from the electron hole pair excited across the band gap. It is assumed that there are a large amount of surface defects which serve as nonradiative recombination paths for the excitation energy in bare ZnS:Mn^{2+} NCs, which will quench the emission of Mn^{2+} to some extent.[11a] By the growth of an additional ZnS shell on ZnS:Mn^{2+} NCs, the surface defects will be greatly reduced; thus, an enhanced emission intensity and lifetime of Mn^{2+} results in ZnS:Mn^{2+}/ZnS core/shell NCs.[10a,26] Note that a similar luminescent enhancement is observed in other core/shell luminescent systems.[27]

4. Conclusions

In summary, high-quality ZnS, ZnS:Mn^{2+}, and ZnS:Mn^{2+}/ZnS core/shell luminescent NCs have been synthesized using a facile method. Self-assembled ZnS NCAs over a large domain are obtained via the increase in viscosity of the reaction medium by the addition of PEG. For ZnS:Mn^{2+} and ZnS:Mn^{2+}/ZnS core/shell NCs, the PL intensity and lifetime of Mn^{2+} are enhanced by the growth of an additional ZnS shell on ZnS:Mn^{2+} due to the elimination of the surface defects. These monodisperse and highly crystalline NCs can be potentially used as labels for biological molecules and active components in optoelectronic devices.

Acknowledgment. This work is financially supported by the "Bairen Jihua" of the Chinese Academy of Sciences, the National Natural Science Foundation of China (50225205, 50572103, 20431030, 00310530, 00610227) and the Ministry of Science and Technology of China (No. 2003CB314707).

Supporting Information Available: TEM images of ZnS, ZnS:Mn^{2+}, ZnS:Mn^{2+}/ZnS, and CdS; synthesis procedure. This material is available free of charge via the Internet at http://pubs.acs.org.

IC061917N

(26) Wang, Z. L.; Quan, Z. W.; Jia, P. Y.; Lin, C. K.; Luo, Y.; Chen, Y.; Fang, J.; Zhou, W.; O'Connor, C. J.; Lin, J. *Chem. Mater.* **2006**, *18*, 2030.

(27) (a) Bai, X.; Song, H.; Pan, G.; Liu, Z.; Lu, S.; Di, W.; Ren, X.; Lei, Y.; Dai, Q.; Fan, L. *Appl. Phys. Lett.* **2006**, *88*, 143104. (b) Wang, Q.; Kuo, Y. C.; Wang, Y. W.; Shin, G.; Ruengruglikit, C.; Huang, Q. R. *J. Phys. Chem. B* **2006**, *110*, 16860. (c) Kompe, K.; Borchert, H.; Storz, J.; Lobo, A.; Adam, S.; Moller, T.; Haase, M. *Angew. Chem., Int. Ed.* **2002**, *42*, 5513.